Gelatine based gel polymer electrolyte towards more sustainable Lithium-Oxygen batteries

Electrochimica Acta 466 (2023) 143026

Contents lists available at ScienceDirect

Electrochimica Acta

journal homepage: www.journals.elsevier.com/electrochimica-acta

Gelatine based gel polymer electrolyte towards more sustainable Lithium-Oxygen batteries

M. Longo, M. Gandolfo, C. Francia, S. Bodoardo, M. Sangermano, J. Amici *

Department of Applied Science and Technology, Politecnico di Torino, Corso Duca degli Abruzzi 24, Torino 10129, Italy

ARTICLE INFO

Keywords:
Lithium-oxygen battery
Gel polymer electrolyte
Photopolymerization
Bio-renewable resources

ABSTRACT

The lithium-oxygen battery has attracted wide interest thanks to its very high theoretical energy density, and as such it is considered by many as a valid battery of the future candidate. However, the challenges in its practical application are many, such as liquid electrolyte evaporation in semi-open systems, as well as solvents instability in a highly oxidizing environment. In this work, we propose to use gelatin, from cold water fish skin, a waste from the fishing industry, to prepare an efficient gel electrolyte for future Li-O_2 battery applications. After a single step methacrylation in water, methacrylated gelatine is directly cross-linked in presence of liquid electrolyte through UV- initiated radical polymerization. The obtained gel polymer electrolytes present good thermal and mechanical properties, good electrochemical stability against Li metal and ionic conductivities as high as 2.51 mS cm^{-1} at room temperature. the Li-O_2 cells assembled with this bio-renewable gel polymer electrolytes were able to perform more than 100 cycles at 0.1 mA cm^{-2}, under constant O_2 flow, at room temperature and at a fixed capacity of 0.2 mAh cm^{-2}. Cathodes post- mortem analysis confirmed that the cross-linked gelatin matrix was able to slow down solvent degradation and therefore enhance the cell reversibility.

1. Introduction

The widespread Li-ion technology, found in most electronic portable devices, presents some intrinsic limitations such as a relatively low energy density, that render it incompatible with the demand for renewable energy storage systems as well as electric vehicles [1–3]. In that sense chemistries, such as Li-O_2 batteries, are considered as promising candidates for future energy storage systems due to the high value of theoretical energy density (estimations range from ≈ 3500 Wh kg^{-1} - to an optimistic ≈ 11000 Wh kg^{-1}) which is close to that of gasoline [4–8]. The enormous value of energy density could be achieved thanks to the usage of O_2 as the active material, which can be directly extracted from air, thus simultaneously reducing the weight and the volume of the batteries [9]. Li-O_2 cells are typically composed of a porous cathode, a nonaqueous organic electrolyte, a separator and metallic Li as the anode. Despite the interesting properties, the commercial applicability of this technology is still unclear due to several, yet unsolved, technical issues. On the anodic side, the reactivity of the Li metal with the liquid electrolyte and the uncontrolled dendrite formation can lead to a reduced cycling stability and result in thermal runaway and explosion hazard [9–12]. The O_2 crossover, that is the diffusion of dissolved O_2 from the cathode to the anode, is another unresolved issue in Li-air batteries, causing the side reaction at the anode, which results in a passivating film on the lithium surface [13]. The presence of a liquid organic electrolyte is one of the drawbacks of this system due to the evaporation, leaking, flammability and degradation in contact with the reactive species produced by the electrochemical reactions [10,14,15]. Furthermore, the presence of even traces of H_2O or CO_2 in the feedstock leads to the generation of electrochemically irreversible species, which in turn lead to higher overpotentials, lower capacity and a reduced electrochemical efficiency [5,16]. To address these issues, research is focused on replacing the liquid electrolytes with gel or semi-solid type electrolytes having similar characteristics and their implementation is widely considered as an ideal pathway. But, despite the attractiveness of the solid-state electrolytes and their excellent mechanical properties, thermal stability and superior safety, they suffer from low ionic conductivity, rarely exceeding 10^{-4} S cm^{-1}, as well as a high interfacial resistance and interfacial contact loss due to the cyclic volume changes of the electrodes [17]. In this sense gel polymer electrolytes (GPE) are a valuable compromise between the high ionic conductivity and good electrolyte/electrode contact presented by liquid electrolytes and the superior mechanical properties and safety of the solid electrolytes. The

* Corresponding author.
E-mail address: julia.amici@polito.it (J. Amici).

https://doi.org/10.1016/j.electacta.2023.143026
Received 28 June 2023; Received in revised form 26 July 2023; Accepted 13 August 2023
Available online 14 August 2023

liquid electrolyte is fixed in the polymeric matrix thus preventing leakage while inhibiting oxygen crossover to the Li anode [17,18]. Furthermore, the flexibility of the GPE enables an easier processability and scalability of the production process with respect to liquid or inorganic solid electrolytes [8]. Numerous GPE systems have been tested, employing a wide range of polymeric matrixes such as polyacrylonitrile (PAN), polyethylene oxide (PEO), polymethylmethacrylate (PMMA), poly(vinylidene fluoride-co-hexafluoropropylene) (PVDF-HFP), polytetrafluoroethylene (PTFE) and NAFION with various results and properties [3,4,17,19–21]. With the implementation of a high efficiency air electrode, Zhao et al. demonstrated a GPE based on PVDF-HFP with $LiClO_4$ and tetraethylene glycol dimethyl ether (TEGDME) as a plasticizer, which presented ultralong cycle life of 553 cycles at a current density of 0.1 mA cm^{-2} and a limited capacity of 0.1 mAh cm^{-2}, and a high ionic conductivity of $3.87 \bullet 10^{-3}$ S cm^{-1} [22]. Despite the good mechanical and electrochemical properties, the implementation of synthetic polymers as the matrix in GPEs is incompatible with the environmental requirements of reduced carbon footprint. In this sense, it is imperative to develop new GPE systems with environmentally friendly and biobased polymers such as cellulose, chitosan and polysaccharides [21,23,24]. Shi et al. produced a sulfonated bacterial cellulose based GPE implementing LiI as a redox mediator presenting an ionic conductivity of $1.6 \bullet 10^{-3}$ S cm^{-1} and a cyclability of 60 cycles thanks to the shuttle-inhibiting properties of the I_3^- ions [25]. Within this frame, in this work we methacrylated gelatin (obtaining GelMA) from cold water fish skin in order to develop a novel GPE, exploiting an UV mediated *in situ* photopolymerization in the presence of 0.5 M LiTFSI in DMSO liquid electrolyte. Gelatin (Gel) is a cheap and abundant natural product which has attracted attention due to its biocompatibility, biodegradability, low production costs and good physical and chemical properties, and is therefore widely used in cosmetics, pharmaceutical and food industries [26,27]. In particular, gelatin can be extracted from cold water fish skin, obtained from the fish industry waste, thus creating an upcycling chain and transferring energy storage solutions within a more circular economy. The obtained membranes presented good thermal and mechanical properties as well as a good electrochemical stability against Li metal. The GelMA10 based GPE also demonstrated an excellent ionic conductivity up to $5.16 \bullet 10^{-3}$ S cm^{-1} at 60°C and $2.51 \bullet 10^{-3}$ S cm^{-1} at 20°C and a full discharge capacity of 8.2 mAh cm^{-2}. The GelMA presence is responsible for the increase in electrochemical performances of the Li-O_2 cell, enabling a stable cycling up until 100 cycles at a limited capacity of 0.2 mAh cm^{-2} and superior rate capability performances.

2. Experimental section

2.1. Materials

Gelatin from cold water fish skin (Gel, average M_n= 60 kDa, CAS 9000-70-8), methacrylic anhydride (MA, M_n= 154.16 g/mol, CAS 760-93-0), sodium hydroxide (NaOH, M_n= 40 g/mol, CAS 1310-73-2), dimethyl sulfoxide (DMSO, M_n= 78.13 g/mol, CAS 67-68-5), lithium bis(trifluoromethanesulfonyl)imide (LiTFSI, M_n= 287.1 g/mol, CAS 90076-65-6) and 2-hydroxy-1-(4-(2-hydroxyethoxy)phenyl)-2-methyl-propan-1-one (Irgacure2959, M_n= 340.32 g/mol, CAS 106797-53-9) were purchased from Sigma-Aldrich and used without further purification unless directly specified.

2.2. Gelatin methacrylation

The methacrylated gelatin (GelMA) was prepared by solubilizing 10 g of Gel in 100 ml of distilled water and heating the solution to 50°C under constant stirring. Once the Gel was completely dissolved, 6 g of MA were added dropwise (0.6 g of MA for 1 g of Gel). The solution was kept under stirring conditions for 4 h at 50°C, keeping the pH at 8 by addition of a 3 M NaOH solution. The resulting product was dialyzed against distilled water for 4 days, replacing the distilled water twice a day, then dried in the oven at 40°C for 3 days and transferred to a vacuum oven for an additional 4 h drying step, at 40°C under vacuum.

2.3. GPE preparation

The GPE production was carried out in an Argon filled glovebox (Mbraun Labstar, Stratham, NH, USA, O_2 and H_2O contents < 0.5 ppm) in order to avoid the radical polymerization inhibition caused by O_2. The precursor solutions were prepared adding different amounts of GelMA (10, 15 and 20 wt%) to a liquid electrolyte solution of LiTFSI 0.5 M in DMSO under constant stirring. Once the GelMA was completely dissolved, 2 wt% photoinitiator Irgacure2959 was added with respect to the GelMA weight. The solutions were then transferred onto a silicon mould and irradiated under UV light (Hamamatsu UV LightningCure LC8 L9588, Hamamatsu, Shizuoka, Japan) with a 100 mW/cm^2 intensity (240-400 nm spectral distribution) for 7 min, obtaining membranes with a thickness of about 400 μm, referred to as GelMA10, GelMA15 and GelMA20.

2.4. Cell assembly

All the electrochemical characterizations that did not require an O_2 flux were carried out employing ECC-Std (EL-Cell, GmbH, Hamburg, Germany) type cells while for the O_2 flux requiring characterizations, ECC-Air (EL-Cell, GmbH, Hamburg, Germany) type cells were used. Li metal chips (15 mm × 0.62 mm, Chemetall s.r.l., Giussano, Italy) and a commercial gas diffusion layer (GDL-24BC, SIGRACET SGL Technologies, Meitingen, Germany) were used as electrodes in the full cell assembly. The GDL-24BC disks were cut in disks (18 mm × 0.235 mm) and dried under vacuum for 6 h at 120°C before use. A commercial glass fibre separator (18 mm × 0.65 mm, ECC1-01-0012-A/L, EL-CELL, Hamburg, Germany) soaked in 400 μl of the liquid electrolyte solution (0.5 M LiTFSI in DMSO) was used as a reference electrolyte (Ref).

2.5. GPE characterization

2.5.1. Physico-chemical characterization

The successful gelatin methacrylation was confirmed via ATR/FT-IR spectroscopy. The analysis was carried out by a Thermo Scientific Nicolet iS50 FTIR Spectrometer (Milan, Italy) between 525 and 2200 cm^{-1} with 32 scans and a resolution of 4 cm^{-1}. The thermal stability of the obtained GelMA and the GPEs was investigated by thermogravimetric analysis (TGA) with a Netzsch thermo-microbalance (TG 209 F3 Tarsus, Selb, Germany) in N_2 in between 25 and 800°C at 20°C min^{-1}. The photorheology tests were carried out with an Anton PAAR Modular Compact Rheometer (Physica MCR 302, Graz, Austria) with a parallel plate configuration (d = 25 mm) and a quartz bottom glass. Photorheometric tests were carried out at room temperature with a 1 Hz shear frequency and a gap value of 1 mm. The time sweep test was performed at an amplitude strain of 1 % and the UV lamp (Hamamatsu UV LightningCure LC8 L9588, Hamamatsu, Shizuoka, Japan) was switched on after 30 s from the start of each test. Mechanical compression tests were carried out by a MTS Systems Corporation dynamometer (MTS QTestTM/10 Elite, Eden Prairie, MN, USA) controlled by a TestWorks 4 software. Cylindrical (d = 9 mm, h = 3.5 mm) GPE samples were tested with a 10 N load cell and a 1 mm min^{-1} compression rate at room temperature.

2.5.2. Electrochemical characterization

The ionic conductivity of the GPEs was investigated by electrochemical impedance spectroscopy (EIS) in the temperature range between 20 and 60°C employing a MKF56 dynamic climate chamber (BINDER GmbH, Tuttlingen, Germany) and a VSP3-e multichannel potentiostat (Biologic, Seyssinet-Pariset, France). The impedance measurements were carried out in the frequency range from 1 to 10^5 Hz at open circuit voltage (OCV), with an amplitude of 0.01 V. The cell setup

used for this characterization consisted of a GPE sandwiched in between two stainless steel blocking electrodes (SS/GPE/SS setup). The value of ionic conductivity at each temperature was computed by the following equation:

$$\sigma = s/(R_b \cdot A) \quad (1)$$

where s is the electrolyte thickness, A is the electrolyte area and R_b is the value of the bulk resistance computed from the intercept at high frequency of the Nyquist plot of the EIS measurement. The electrochemical stability window was investigated through linear sweep voltammetry (LSV) using a SS/GPE/Li cell setup. The LSV was carried out with a CHI660D Electrochemical Workstation (CH Instruments, Inc, Austin, TX, USA) in the potential interval between 2.5 and 4.5 V (*vs* Li^+/Li) with a 0.1 mV s^{-1} scan rate. The interfacial stability of the GPEs was investigated by EIS carried out every day for 30 days on a Li/GPE/Li symmetric cell, to evaluate the increase of impedance caused by the reactivity of the GPE with the Li metal at OCV. The Li-ion transference number (t_{Li^+}) was determined through EIS performed on a Li/GPE/Li symmetric cell before and after a chronoamperometry, with an applied potential of 10 mV over the OCV. The value of t_{Li^+} was computed from the following equation:

$$t_{Li^+} = \frac{I_s \cdot (\Delta V - I_0 R_0)}{I_0 \cdot (\Delta V - I_s R_s)} \quad (2)$$

where ΔV is the applied potential (10 mV), I_0 and I_s are the initial and steady-state currents and R_0 and R_s are the initial and steady-state interfacial resistance respectively. A plating and stripping test was carried out on the GPEs to evaluate Li^+ ion transport through the electrolyte in a Li/GPE/Li symmetric cell, by BT-2000 battery tester (Arbin Instruments, College Station, TX, USA). The constant current density was 0.1 mA cm^{-2}, considering a 18 mm electrode area, for 500 cycles. For each step, the time was set at 1 h and the voltage limits were ± 5 V. For the full cell tests a GDL-24BC/GPE/Li cell setup was employed, using the ECC-Air cells (EL-Cell, GmbH). The cells were rested under O_2 flow for 6 h at OCV and then cycled between 2 and 4.5 V (*vs* Li^+/Li) under a 4 ml min^{-1} O_2 flow at 0.1 mA cm^{-2} with the BT-2000 battery tester (Arbin Instruments). The most promising GPE was selected to carry out the full cell tests.

2.5.3. Post-mortem characterization

In order to investigate the presence of crystalline phases of the discharge products deposited in the cathode porosities, a *post-mortem* XRD analysis was carried out using a high-resolution Philips X'pert MPD powder diffractometer (Philips, Amsterdam, The Netherlands). The diffractometric analysis was carried out between 10 and 90° with a Cu Kα radiation (V = 40 kV, I = 30 mA). The *post-mortem* analysis was carried out on discharged cathodes obtained by disassembling cells containing both GelMA10 and the liquid electrolyte. The results were compared to a pristine GDL-24BC cathode. The discharge and charge products morphologies present in the cathode porosities, as well as the pristine GDL morphology, were investigated by means of a Field Emission Scanning Electron Microscope (FESEM, ZEISS Supra 40, Oberkochen, Germany).

3. Results

3.1. Physico-chemical characterization

Gelatin (Gel) was methacrylated following a previously reported experimental procedure, in order to enable the UV-mediated radical polymerization to obtain a cross-linked membrane [28], the reaction is schematized in Fig. 1. The successful methacrylation of the Gel into GelMA was confirmed via ATR/FTIR spectroscopy, the corresponding Gel and GelMA spectra are reported on Fig. 2.a. The characteristic peaks of the methacrylic group should be evident at 1640 cm^{-1}, but in this case, they are completely covered by the more intense amide I peptide C=O stretching peak of the backbone gelatin located at 1645 cm^{-1}. Therefore, the methacrylic C=C double bonds was verified by the presence, on the GelMA spectrum, of two peaks at 860 and 930 cm^{-1} (Fig. 2.a) relative to the C-H stretching of the C=C double bond [27,29]. The thermal stability of Gel and GelMA, along with the photocured gelatin-based gel polymer electrolytes, was investigated by thermogravimetric analysis and the results are reported in Fig. 2.b. Both Gel and GelMA showed an initial weight loss of about 10% in the temperature range between 40 and 200°C due to the loss of residual water molecules retained in both the Gel and GelMA structures, even after vacuum drying of the samples. This water molecules are released from the samples at different temperature intervals (from 40 up to around 160°C) depending on the type of interaction they have with the gelatin backbone chain [30]. The temperatures at which water is released from the GelMA are lower than those of the Gel, indicating a decrease in water affinity with the methacrylation and, therefore, less water bound through hydrogen or polar interactions. The onset temperatures (defined as the

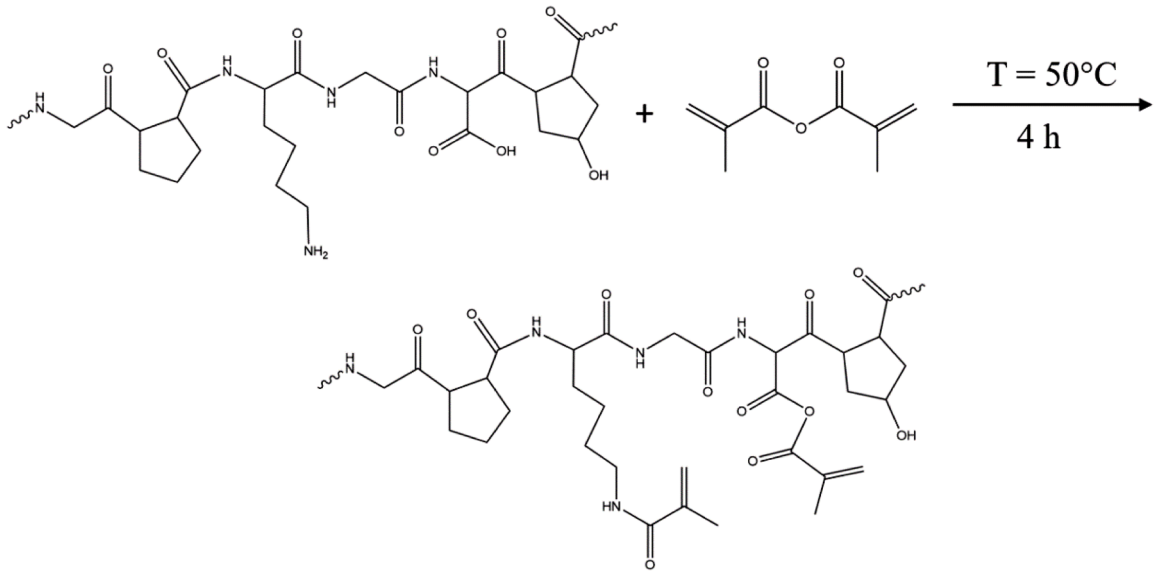

Fig. 1. Gelatin methacrylation reaction.

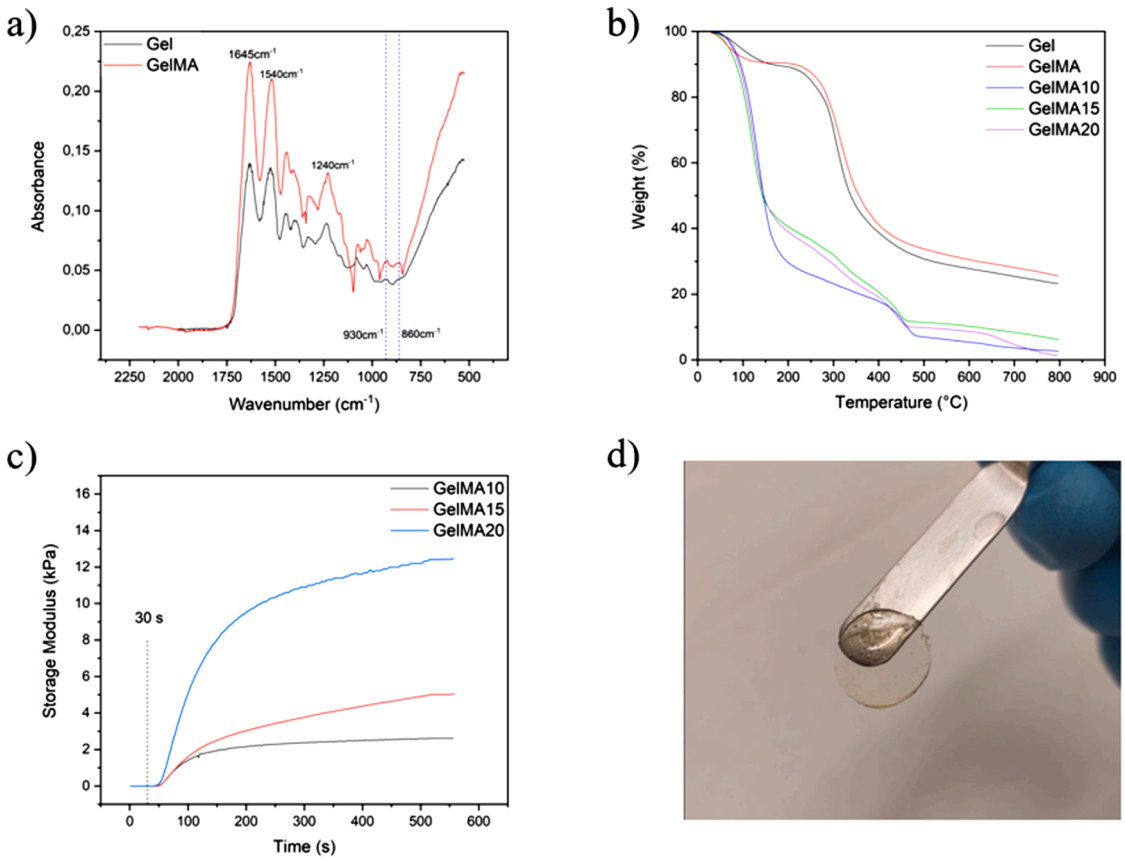

Fig. 2. a) FT-IR spectra of Gel and GelMA. b) Thermogravimetric curves of Gel, GelMA and the photocured membranes. c) Photorheometric curves of the GPEs. d) Picture of the GelMA10 membrane.

temperature at which the sample has lost 2% of its original weight) for the water elimination process are 50 and 65.5°C respectively for GelMA and Gel, thus indicating a stronger water affinity of the Gel structure, due to the presence of a higher concentration of polar groups (NH_2 and OH groups). The second degradation step occurs between 200 to 400°C for both Gel and GelMA and is referred to the degradation of the polymer chains sporting a weight loss of about 60%. The DTG plot (Fig. S1) allows to determine the temperatures at which the maximum degradation rate is recorded, corresponding to 306.5 and 318°C respectively for Gel and GelMA. The residual weight remaining at the end of the analysis accounts for 23.13 and 25.51% for Gel and GelMA, respectively. After confirming the successful methacrylation of the gelatin and verified the thermal stability of GelMA, its photoreactivity was investigated. To this end, a photorheological analysis was carried out, varying GelMA content in DMSO, and following the polymerization process through the increase of the storage modulus. Three different precursor formulations were prepared, one containing 10 wt% of GelMA in DMSO (referred to as GelMA10), one containing 15 wt% (referred to as GelMA15) and one containing 20 wt% (referred to as GelMA20). The obtained results are reported in Fig. 2.c. The polymerization reaction of the methacrylated gelatin formulations under UV light presents an induction time of 20 s for GelMA10 and GelMA15, and of 15 s for GelMA20. The shorter induction time for GelMA20 can be due to the higher concentration of GelMA and, therefore, of methacrylic double bonds resulting also in a higher polymerization rate (obtained from the photorheology curve slope) and in a higher G' plateau. Moreover, the GelMA20 sample requires the longest time to reach the G' plateau attested at 12.45 kPa, after 520 s of irradiation. For GelMA10 and GelMA15 the plateau was reached after 475 and 510 s of irradiation and the values of the G' plateau were 2.61 and 5 kPa respectively, showing an increase of the storage modulus by increasing the polymer content in DMSO, as expected. These last results confirm the possibility to obtain cross-linked GelMA membranes in DMSO. At this point, the polymerization was performed in DMSO containing 0.5 M of LiTFSI, to obtain a UV-cured organogel polymer electrolyte with sufficient Li ion conductivity. The GelMA content varied as previously described, and the obtained gel polymer electrolytes are referred to as GelMA10, GelMA15 and GelMA20. The polymerization is carried out in a circular silicon mold and the obtained samples are transparent and self-standing (Figs. 2. d and S2). First of all, the thermal stability of the obtained GPEs was assessed, the corresponding thermograms are reported on Fig. 2.b. As can be observed, the degradation profiles of the three samples show two main steps. The first one (about 80-90%) occurs in the temperature interval between 50 and 200°C and is caused by the DMSO evaporation (T_{eb} = 189°C) with onset temperatures of 63.9, 53.1 and 59.8°C for GelMA10, GelMA15 and GelMA20 respectively. The GelMA chains degradation starts at around 400°C for the GPEs with a maximum rate achieved at 454.7, 444.9 and 437.1°C for GelMA10, GelMA15 and GelMA20 respectively. Another contribution in this degradation step is the LiTFSI degradation at 450°C [31]. The increase in degradation resistance of the polymeric matrix of the GPEs with respect to the GelMA structure can be ascribed to the presence of crosslinked polymer chains, that are absent in the GelMA powder. These results show that the GelMA based GPEs can be a possible candidate for a safe gel electrolyte in Li-air systems since, in case of DMSO evaporation, and subsequent diffusion through the porous cathode, the cell would be left with a polymeric matrix presenting a good thermal stability, thus avoiding dramatic short circuit, even at high temperatures. Another fundamental aspect, to avoid short circuit and guarantee cell safety, regards the electrolyte mechanical properties. In this work, the mechanical properties of the UV cured membranes were investigated by means of a compression test reported in Fig. S3. The compressive modulus was computed from the linear

elastic region for each GPE. The values of the computed moduli are 11.57, 20.77 and 30.96 kPa for GelMA10, GelMA15 and GelMA20 respectively, demonstrating a linear trend reported in Fig. S4. Interestingly, as concern the physico-chemical characterizations, no negative interactions between DMSO and GelMA were recorded, since both the compressive and the storage moduli evaluated in this work are comparable with the values of GelMA based hydrogels moduli [31–33,31,34]. Therefore, no negative influence of the DMSO on the mechanical or photorheologic properties was found.

3.2. Electrochemical characterization

In order to check if the biobased organogels could be indeed used as GPEs in Li-based batteries, the ionic conductivity (σ) of the organogels was determined by EIS using a symmetric SS/GPE/SS cell, in the temperature range between 20 and 60°C, and the obtained results are reported in Fig. 3.a. The linear trend highlighted in the plot stems from the Arrhenius-like Li^+ ions transfer mechanism which is dominated by the ionic diffusion through the liquid electrolyte in the gel structure [35]. The UV cured membranes demonstrate a good ionic conductivity, ascribed to the high percentage of liquid electrolyte, reaching the values of 5.16 mS cm^{-1}, 4.74 mS cm^{-1}, 3.91 mS cm^{-1} at 60°C and 2.51 mS cm^{-1}, 2.2 mS cm^{-1} and 1.66 mS cm^{-1} at 20°C for GelMA10, GelMA15 and GelMA20 respectively, considering a membrane diameter of 18 mm. The values of conductivity are about two orders of magnitude above the values usually measured with polymer electrolytes and comparable with the conductivity of liquid electrolytes [9,10,15,36–38], thus confirming the Li^+ ion diffusion-based conduction mechanism hypothesis. The increase in the GelMA concentration of the formulations has the effect of decreasing the ionic conductivity but the linear behaviour of the plot is conserved, so that the diffusion-based charge transfer can be considered as the only conduction mechanism at all the investigated temperatures.

Another important parameter for a GPE is its electrochemical stability window (ESW). This is particularly true in the case of the Li-air application, as the potential range is quite wide (from 2 to 4.5 V *vs* Li^+/Li), hence potentially causing the electrolyte degradation at high potentials. Therefore, LSV was performed on the three considered samples focusing only on the anodic branch of the potential, that is in the range between 2.5 and 4.5 V. The obtained results were compared to a reference cell containing the same liquid electrolyte soaked in a commercial glass fibre separator (referred to as Ref). As shown in Fig. 4.a all the GPEs, as well as the reference electrolyte, are electrochemically stable in battery operational voltage interval, thus confirming the absence of reactions between the GPEs and lithium in the potential range of interest. For lithium containing electrochemical systems, one essential property of the electrolyte is the long-term stability against the metallic lithium [15]. To assess the long-term interfacial stability of the GelMA based GPEs, impedance measurements were conducted at OCV on a Li/GPE/Li cell for a period of one month. The resulted Nyquist plots for the three formulations are given in Fig. 3.b, c and e. As it can be noted, the charge-transfer (R_{ct}) resistance values, corresponding to the semi-circle diameter, show a slight fluctuation in the GelMA10 and GelMA15 plots (Fig. 2.b and 2.c), of about ±20 Ω, which is small enough to consider the GPEs stable in contact with the Li metal electrodes. As for the GelMA20 (Fig. 3.d), R_{ct} values, as well as the bulk resistance R_b, are consistently increasing, therefore demonstrating a reduced stability against Li metal. This increase in interfacial resistance can be caused by a large quantity of residual water in the membrane, due to the larger Gel percentage, as well as an incomplete drying of the powders. The lithium-ion transference numbers (t_{Li^+}) were computed for each GPE using Eq. (2) and are reported in Fig. 4.b, c and d. The transference number is a crucial measure in the characterization of electrolytes as higher transference numbers are associated with a reduced concentration polarization at the electrode/electrolyte interface caused by the accumulation of the

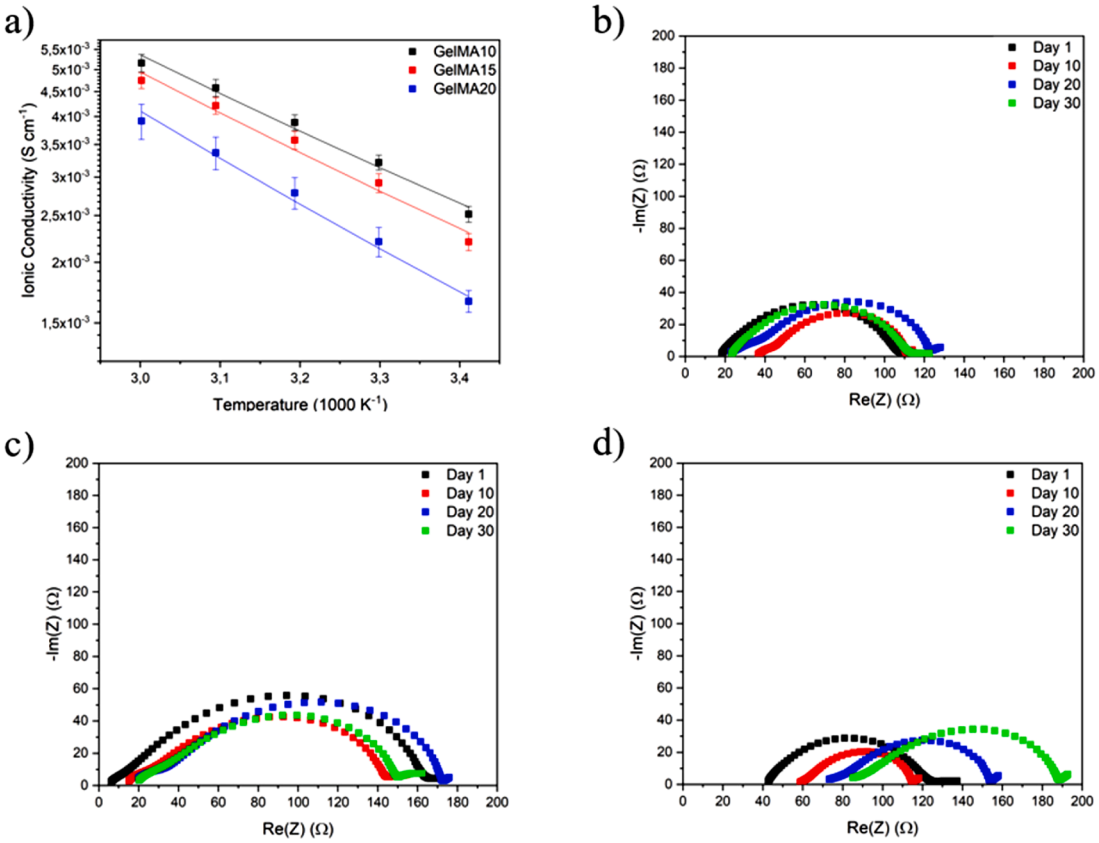

Fig. 3. a) Arrhenius plot of the GPEs. Time evolution of EIS for b) GelMA10. c) GelMA15. d) GelMA20.

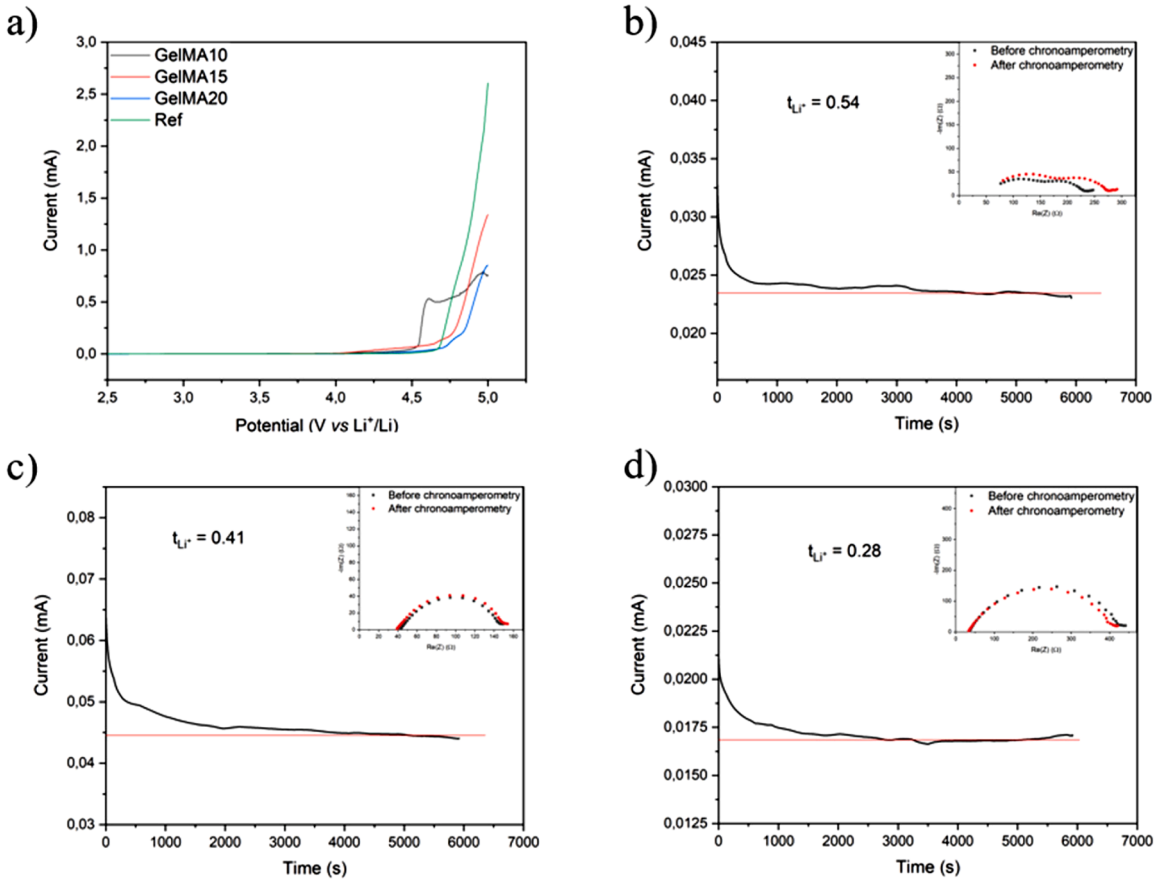

Fig. 4. a) Electrochemical stability window of the GPEs and the reference electrolyte. Chronoamperometry of a) GelMA10. b) GelMA15. c) GelMA20, the inserts show the Nyquist impedance before and after polarization.

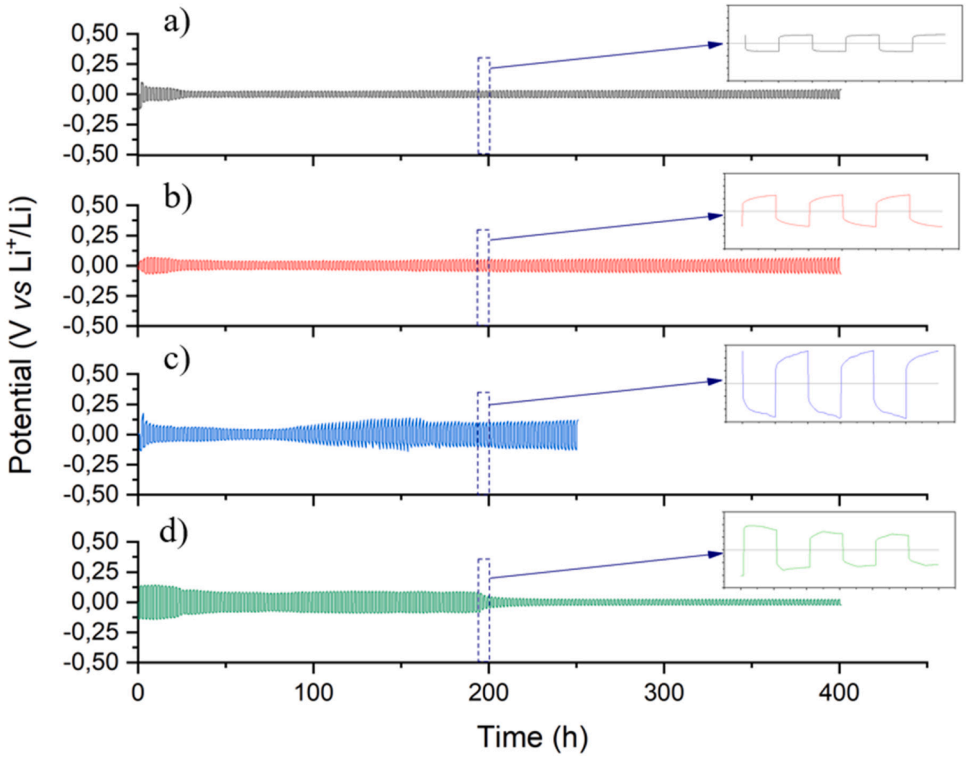

Fig. 5. Polarization curves of Li/Li symmetrical cells containing a) GelMA10. b) GelMA15. c) GelMA20. d) Reference cell.

present ions. Such smaller polarization favours the homogeneous deposition of metallic lithium on the anode surface, thus hindering dendrites nucleation and growth [39]. The obtained values of t_{Li^+} for the GPEs are 0.54, 0.41 and 0.28, respectively for GelMA10, GelMA15 and GelMA20. Such t_{Li^+} values stem from the presence of a considerable amount of liquid electrolyte in the gel polymer membranes and the polymer chains relaxation due to the polymer solvation [40]. These results show comparable t_{Li^+} values with respect to the reference cell, sporting a t_{Li^+} of 0.54 (Fig. S5), as well as other gel polymer electrolytes or liquid-based ones found in literature [13,15,41]. It is also clear that the transference number is directly correlated with the amount of liquid electrolyte, demonstrating an almost linear trend shown in Fig. S6. The reversibility of the Li^+ transport across the electrolyte, as well as the cycling stability, were characterized by a galvanostatic plating and stripping test on symmetric Li/Li cells containing the GPEs and the reference liquid electrolyte. The measurements were conducted with a current density of 0.1 mA cm^{-2} and a time step limit of 1 h at room temperature. As shown in Fig. 5.a and b the cells containing the GelMA10 and GelMA15 membranes present a stable cycling profile and a low overpotential of 37 mV and 68 mV respectively after 400 h of cycling, which is comparable to the overpotential of the reference cell of 22 mV. The small polarization of the Li/Li cells containing the GelMA10 and GelMA15, as well as the stable cycling up to 400 h without cell failure, demonstrate a superior compatibility with lithium metal. The cycling profile of the cell sporting GelMA20 as the GPE, shown in Fig. 5. c, has a sharp increase from the 70th hour of cycling reaching 138 mV after 150 h and present a continuous polarization indicating a certain instability in contact with the metallic Li electrodes, in accordance with the previous characterizations. The reference cell (Fig. 5.d), on the other hand, displays an initial higher overpotential possibly due to the SEI creation. After the drop in the voltage profile around the 200th hour of cycling, the cell continues to cycle stably for other 200 h with a low overpotential. Considering the voltage profiles, the GelMA10 cell maintains a flat plateau up until 400 h which is indicative of a favoured Li^+ deposition and dissolution with a low energy barrier [42]. In the GelMA15 and, more significantly, in the GelMA20 voltage profiles, on the other hand, the overpotentials are constantly increasing with a curved shape. This arched profile stems from the accumulation of dead lithium on the electrode surface and the thickening of the SEI layer [42]. Considering the results of the physico-chemical and electrochemical characterizations, the GelMA10 electrolyte presents the best electrochemical properties, such as ionic conductivity and electrochemical stability window, while still displaying good mechanical and thermal stability, and hence it has been chosen for the further full cell testing. The lithium oxygen cells were assembled with either the GelMA10 GPE or the reference glass fibre soaked with LiTFSI 0.5 M in DMSO liquid solution as the electrolyte, the commercial GDL24BC as the gas electrode and lithium metal as the anode. The galvanostatic discharge curves for GelMA10 and the reference cell at a current density of 0.1 mA cm^{-2} are shown in Fig. 6.a. The GelMA10 cell present a voltage plateau at 2.75 V and a superior specific discharge capacity of 8.2 mAh cm^{-2} with the reference cell reaching 5.7 mAh cm^{-2} at the same voltage. This value of the initial specific discharge capacity is comparable with other result reported in literature, as it is shown in Table.S1 [43–46]. To further probe the electrochemical properties of the GelMA10 electrolyte, the galvanostatic charge and discharge curves at different current densities with a fixed areal capacity of 0.5 mAh cm^{-2} are shown in Fig. 6.b and c. As the current density increases from 0.05 mA cm^{-2} to 1 mA cm^{-2}, the charge/discharge voltage profile of the reference cell shows an evident instability with the overpotential increasing from 1.41 V at 0.05 mA cm^{-2} to 2.5 V when cycled at 0.5 mA cm^{-2}, shown in Fig. 6.d. In contrast, charge/discharge profiles of the GelMA10 containing cell are

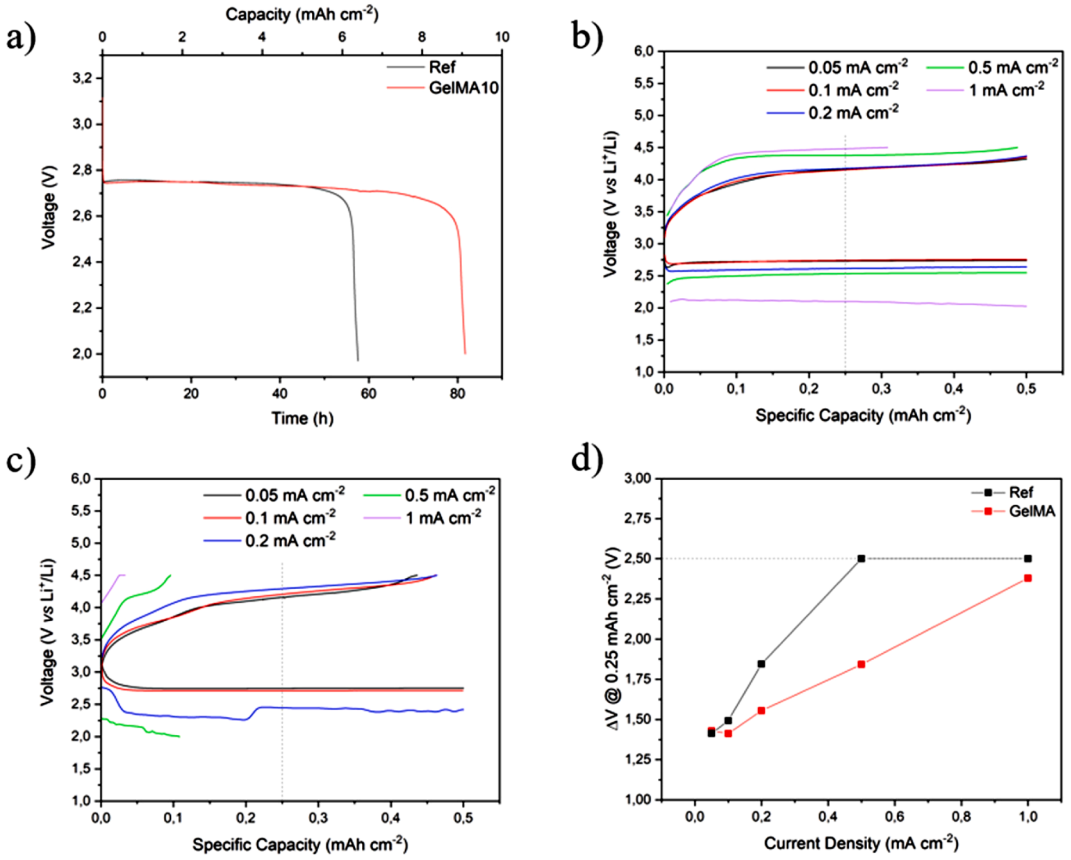

Fig. 6. a) Full discharge curves for GelMA10 and reference cell. Charge and discharge curves at different current densities of b) GelMA10 and c) Reference cell. d) Overpotential variation at a constant specific capacity.

more stable with a limited increase in overpotential and a reversible charge and discharge cycling at higher current rates. In fact, the GelMA10 containing cell is able to reversibly cycle at the highest current density of 1 mA cm^{-2} with a significantly lower overpotential with respect to the reference cell. The better performances at high current densities can be ascribed to the penetration of the GelMA based membrane into the cathode porosities, thus increasing the extent of the active triple-phase interface from just the surface of the GDL to the volume of the air cathode [44]. To obtain a deeper understanding of the charge and discharge behaviour of the GelMA10 containing cell, EIS measurements were conducted on a GDL24BC/Li full cell after the discharge and recharge, as well as on a fresh one left in an O_2 atmosphere for 6 h. The galvanostatic charge and discharge were conducted with a current density of 0.1 mA cm^{-2} and a limited areal capacity of 0.5 mAh cm^{-2}. The results of the EIS measurements, as well as the equivalent circuits obtained by means of ZView software, are reported in Fig. S7.a-b while the values of R_b, R_{if} and R_{ct} are reported in Tab.S2. After the first discharge of the pristine cell, the charge transfer resistance R_{ct} increases from an initial 113.7 Ω to 133.4 Ω, in accordance with the formation of insulant discharge products in the porosities of the GDL. After the charge process, the R_{ct} drops from 133.4 Ω to 63.2 Ω, demonstrating the reversible decomposition of the discharge products. The decrease of the interfacial resistance R_{ct} after the charge process can be ascribed to the formation of stable and conducting interfacial layers both on the anode and the cathode, as well as the deep infiltration of the GPE in the cathode [40,44]. The stabilized interfacial layer formed after the discharge process is responsible for the better cycling performances of the GelMA10 containing cell, due to the instauration of a mainly horizontal lithium deposition which reduces the impact of lithium volume changes during cycling [47]. The EIS measurements were again carried out after the 5th discharge and recharge processes with the R_{ct} values of 131.6 Ω and 61.8 Ω. This result is indicative of the superior cyclability and reversibility of the electrochemical reactions in the GelMA10 containing cell. Considering the reference cell, the interfacial resistance R_{ct} increases significantly from 113.6 Ω to 289.5 Ω, demonstrating a more significant deposition of non-reversible reaction products blocking the charge transfer at the interface [43,48]. Furthermore, after the first recharge the interfacial resistance R_{ct} drops to 70.7 Ω which is slightly higher than the value exhibited by the GelMA10 containing cell, but after 5 cycles the R_{ct} after the charge process increases up to 85.9 Ω. This demonstrates the lower reversibility of the electrochemical reactions in the reference cell that results in the accumulation of electrochemically irreversible species in the cathode. This is also confirmed by XRD analysis carried out on the cathodes of the GelMA10 and the reference cell before and after cycling (Fig. 7.a-b). The presence of LiOH peaks in the reference cell spectra both after discharge and charge is in line with the hypothesis of a less reversible cycling of the liquid electrolyte, with the possible DMSO degradation in contact with the cell discharge products. In the spectrum of the charged GelMA10 cathode only the pristine GDL24BC peaks are visible demonstrating either a complete electrochemical reversibility of the deposited Li_2O_2 or the presence of amorphous species deposited in the cathode pores during discharge. To further evaluate the presence and the morphology of the discharge products, SEM images of the cathodes before and after cycling at a 0.1 mA cm^{-2} current density were collected. Fig. S8.b shows the presence of an evenly distributed and mainly amorphous layer of products deposited in the cathode porosities which can be associated to poorly crystalline "film-like" Li_2O_2, as already reported in different works [49]. Indeed, it has been shown that the "film-like" Li_2O_2 morphology could be generated through a surface-growth mechanism, favoured in solvents such as DMSO during cycling at high current densities (0.1 mA cm^{-2}). The cathode in the GelMA10 containing cell completely recovers the pristine morphology after the charge process (Fig. S8.c), demonstrating a good reversibility of the galvanostatic cycling of the cell, probably thanks to a higher contact area between the surface of the cathode and the "film--like" conformation of the discharge products, enhancing the transfer of electrons and therefore the reversibility of such products [50–52]. Conversely, the reference cell cathodes (Fig. S8.d-f) display a significant deposition of discharge products that completely cover all cathode porosities. After the charge process the residual presence of large crystalline LiOH particles (about 1 μm in diameter), also detected by XRD, confirm the lower reversibility of the electrochemical reactions in the liquid reference electrolyte. The galvanostatic charge/discharge profiles for a GelMA10 cell, as well as the reference one, cycled with a current density of 0.1 mA cm^{-2} at a limited capacity of 0.5 mAh cm^{-2} are reported in Fig. 8.a and b. The GelMA10 charge and discharge profiles are stable, and the cycling process is reversible up until the 20th cycle as shown in Fig. 8.a, which corresponds to a lifespan of 200 h. In contrast, the reference cell voltage profiles, reported in Fig. 8.b show an unstable cycling with the cell failing after 10 cycles. The superior stability of the GelMA10 is further displayed in Fig. S9 with a decrease of the overpotential over the 20 cycles. On the contrary, the reference cell shows an increase in overpotential starting from the 5th cycle. In this case the overpotential was computed as the difference between the charge and discharge voltage values at a fixed capacity of 0.25 mAh cm^{-2}. The GelMA10 overpotential remains quite stable around 1.3 V, presenting a slight decrease reaching 1.21 V after 10 cycles, due to the formation of a fully stable SEI that enables a more reversible operation. Considering the reference, the continuous cell polarization brings the overpotential to reach 2.5 V after 10 cycles demonstrating the constant accumulation of dead lithium and thickening of the SEI at the anode side and the poor reversibility of the discharge products at the cathode side. The capacity retention plots for the galvanostatic cycling of the two cells, at the limited capacity of 0.5 mAh cm^{-2}, as well as the Columbic efficiency, are reported in Fig. 8.c and d. The GelMA10 cell presents almost constant specific charge and discharge capacities of 0.5 mAh cm^{-2} for all the 20

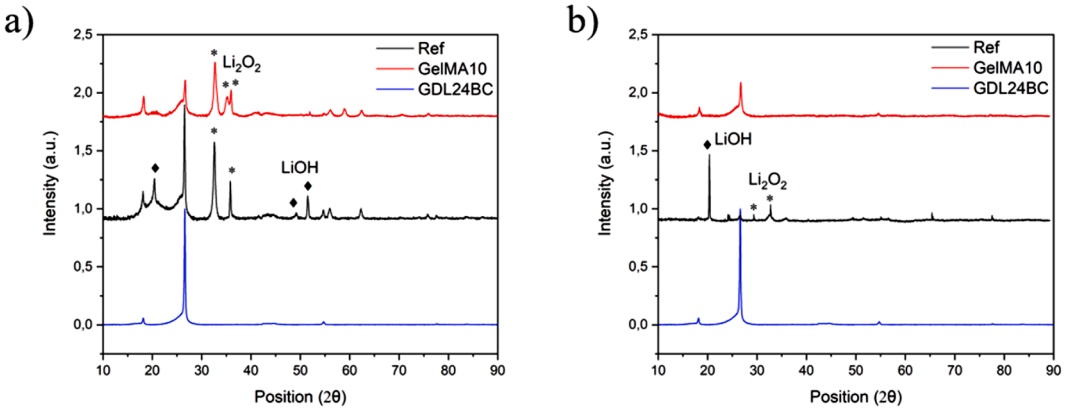

Fig. 7. XRD spectra of cathodes of GelMA10 and reference cells after a) discharge. b) charge.

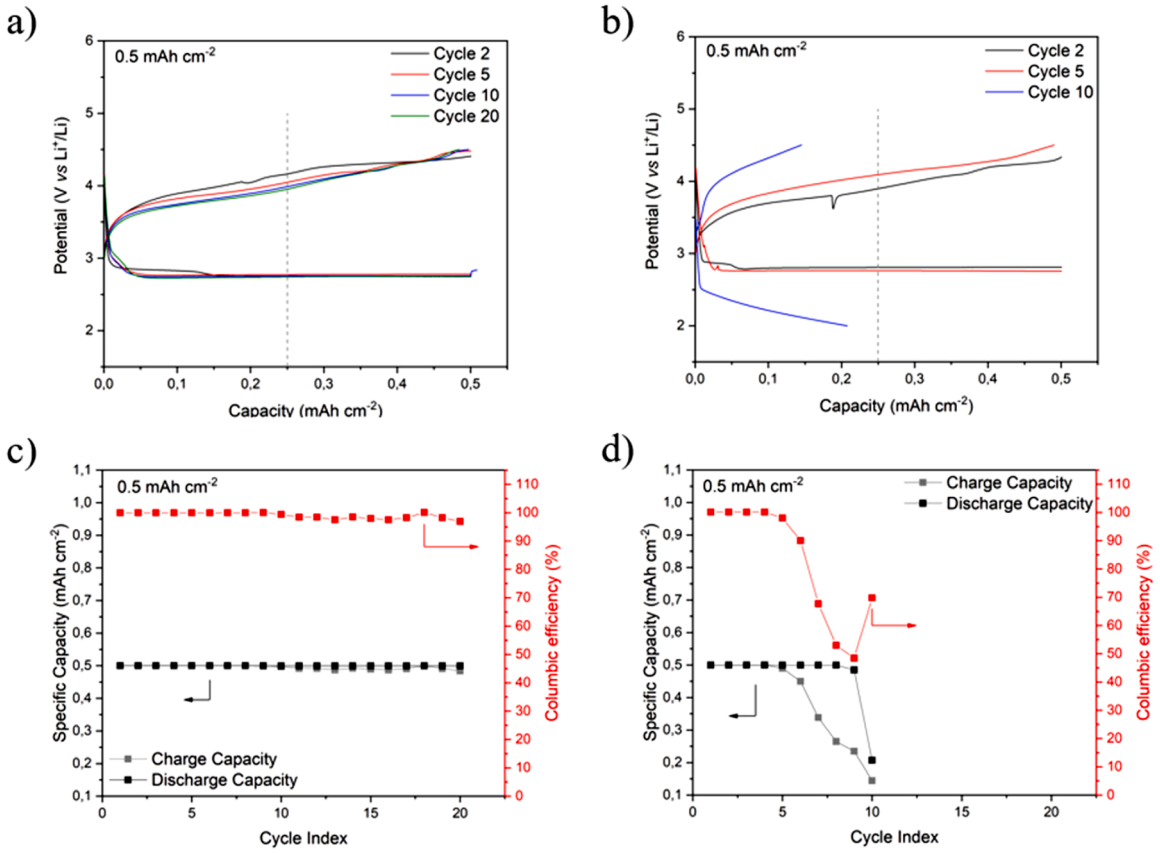

Fig. 8. Voltage profiles for the cycling of a) GelMA10. b) Reference cell. Capacities retention and Columbic efficiency plots for a) GelMA10. b) Reference cell with a 0.5 mAh cm^{-2} fixed capacity.

cycles with a Columbic efficiency of 99.06% ± 0.24 while the reference cell displays a lower Columbic efficiency of 82.43% ± 4.44. The more stable cycling performances displayed by GelMA10 containing cells is probably a consequence of the significative presence of electron-rich C=O groups that are shown to spontaneously adsorb on the GDL substrate, causing a more homogeneous Li^+ flux and an even nucleation of electrochemically reversible Li_2O_2 [53]. In order to test the extent of the electrochemical properties of GelMA10, as well as the capacity retention over longer cycling, the same test was carried out at a lower limited capacity of 0.2 mAh cm^{-2}. The GelMA10 containing cell voltage profiles are shown in Fig. 9.a. They present a reversible behaviour up until 100 cycles with a constant overpotential, computed as the difference between the voltage during charge and discharge at a capacity of 0.1 mAh cm^{-2} (Fig. S10). The overpotential of the GelMA10 cell increases from 1.35 V in the first cycle to 1.45 V in the 23rd one, but after it decreases again to 1.41 V remaining stable up to the 100th cycle and thus demonstrating the good electrochemical stability of the GelMA10 membrane, even for longer working times. After the 100th cycle the cell continues to cycle, albeit with a reduction in the reversibility of the electrochemical reactions. The voltage profiles of the reference cell in Fig. 9.b, in contrast, display a much more unstable behaviour. The reference cell demonstrates a reversible cycling up until the 20th cycle, as shown in Fig. 9.d, followed by a severe increase in the overpotential up to 2.5 V, and consequently, a drop in the charge capacity after 40 cycles. In Fig. 9.c and d the charge and discharge capacities are reported for both cells. The charge capacity for GelMA10 is slightly more unstable with respect to the fixed 0.5 mAh cm^{-2} cycling one, due to the longer working time. Nonetheless, the GelMA10 cell presents an almost total capacity retention up to the 100th cycle, which result in a Columbic efficiency of 98.28% ± 0.11, in contrast to the 80.33% ± 2.09 of the reference cell. The GelMA10 cell continues to cycle reversibly up until the 120th cycle with a slight instability in the charge capacity, resulting in a Columbic efficiency of 97.68% ± 0.14, however after the 120th cycle the charge capacity experiences a drop implying the degradation of the cell components.

4. Conclusions

In this work a biobased gel polymer electrolyte was fabricated via a fast, cheap and green UV-mediated photopolymerization of methacrylated gelatin in a typical liquid electrolyte. The methacrylation of the gelatin was conducted via a one-step reaction and its success was asserted via FT-IR spectroscopy. GelMA10 membranes displayed good stability against Li metal and an electrochemical stability window comparable to the liquid electrolyte reference, while sporting the appealing value of room temperature ionic conductivity of 2.51 mS cm^{-1}. Lithium symmetrical cells containing GelMA10 electrolytes showed low overpotentials and stable cycling performance, being highly compatible with Li metal, while the discharge capacity of the GelMA10 cell was found to be 8.2 mAh cm^{-2}. The improved interface with Li metal and the expanded triple-phase reaction zones in the air cathode result in the reduced interfacial resistance and the superior electrochemical performances of the GelMA10. Thus, GPE showed a more reversible cycling both in a wider current density range and for longer galvanostatic cycling, achieving more than 100 cycles at a 0.2 mAh cm^{-2} limited capacity. In conclusion, this study demonstrates that encouraging results can be obtained employing a fully green and renewable resource as the gelatin, a waste of the fishing industry, to prepare an efficient gel electrolyte for future Li-O_2 battery applications.

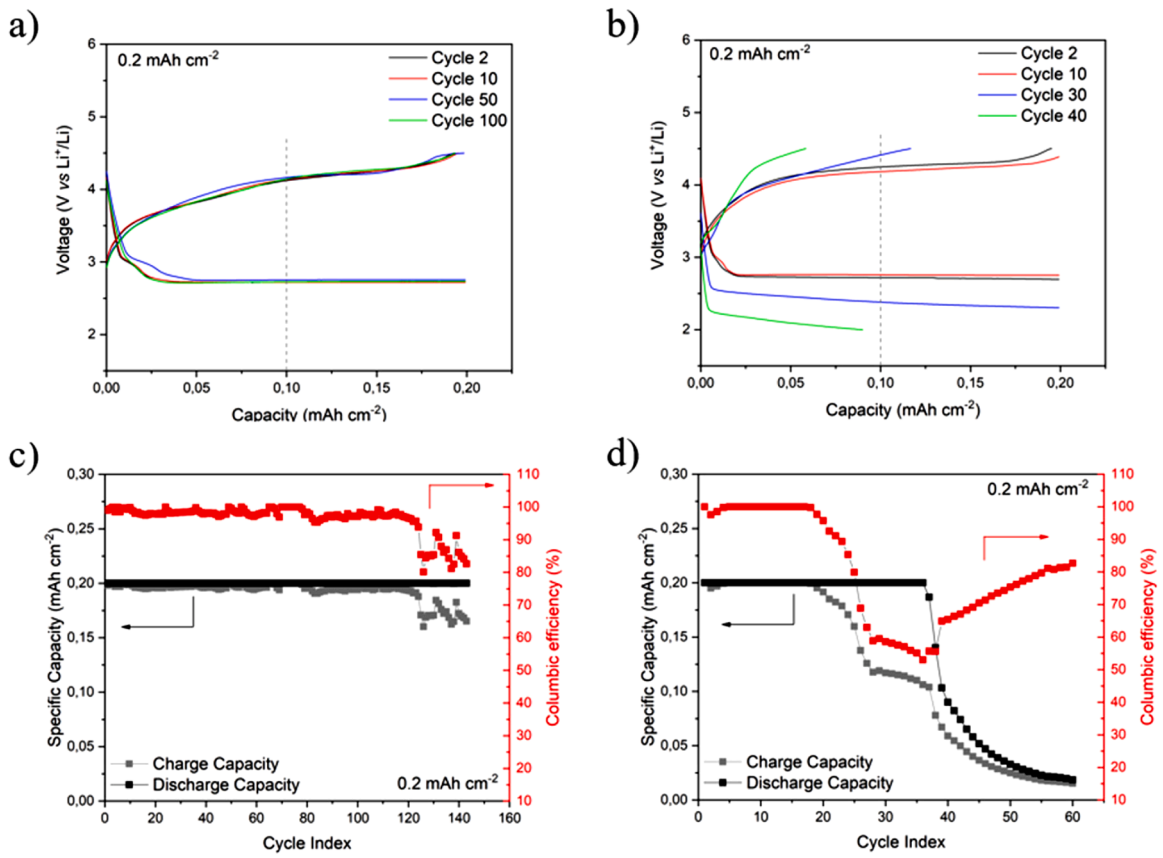

Fig. 9. Voltage profiles for the cycling of a) GelMA10. b) Reference cell. Capacities retention and Columbic efficiency plots for a) GelMA10. b) Reference cell with a 0.2 mAh cm^{-2} fixed capacity.

CRediT authorship contribution statement

M. Longo: Methodology, Investigation, Data curation, Writing – original draft. **M. Gandolfo:** Methodology, Investigation, Data curation. **C. Francia:** Writing – review & editing. **S. Bodoardo:** Writing – review & editing, Funding acquisition. **M. Sangermano:** Conceptualization, Methodology, Writing – review & editing. **J. Amici:** Conceptualization, Methodology, Data curation, Writing – review & editing, Funding acquisition.

Declaration of Competing Interest

The authors declare that they have no known competing financial interests or personal relationships that could have appeared to influence the work reported in this paper.

Data availability

Data will be made available on request.

Acknowledgement

This work was funded by "Piano triennale di realizzazione 2022-2024 della ricerca di sistema elettrico nazionale, Progetto integrato: tecnologie di accumulo elettrochimico e termico", PTR 22-24 (MISE ENEA)

Supplementary materials

Supplementary material associated with this article can be found, in the online version, at doi:10.1016/j.electacta.2023.143026.

References

[1] P. Chen, F. Bai, J. wen Deng, B. Liu, T. Zhang, Recent progresses and challenges in aqueous lithium–air batteries relating to the solid electrolyte separator: A mini-review, Front. Chem. 10 (2022), https://doi.org/10.3389/fchem.2022.1035691.
[2] N. Imanishi, O. Yamamoto, Perspectives and challenges of rechargeable lithium–air batteries, Mater. Today. Adv. 4 (2019), https://doi.org/10.1016/j.mtadv.2019.100031.
[3] U.R. Farooqui, A.L. Ahmad, N.A. Hamid, Challenges and potential advantages of membranes in lithium air batteries: A review, Renew. Sustain. Energy. Rev. 77 (2017) 1114–1129, https://doi.org/10.1016/j.rser.2016.11.220.
[4] M. Celik, A. Kızılaslan, M. Can, T. Cetinkaya, H. Akbulut, Electrochemical investigation of PVDF: HFP gel polymer electrolytes for quasi-solid-state Li-O2 batteries: effect of lithium salt type and concentration, Electrochim. Acta 371 (2021), https://doi.org/10.1016/j.electacta.2021.137824.
[5] J.H. Kang, J. Lee, J.W. Jung, J. Park, T. Jang, H.S. Kim, J.S. Nam, H. Lim, K. R. Yoon, W.H. Ryu, I.D. Kim, H.R. Byon, Lithium-air batteries: Air-breathing challenges and perspective, ACS. Nano 14 (2020) 14549–14578, https://doi.org/10.1021/acsnano.0c07907.
[6] Y. Lu, S. Tong, F. Qiu, J. Jiang, N. Feng, X. Zhang, P. He, H. Zhou, Exploration of LiO2 by the method of electrochemical quartz crystal microbalance in TEGDME based Li-O2 battery, J. Power. Sources 329 (2016) 525–529, https://doi.org/10.1016/j.jpowsour.2016.08.117.
[7] X.F. Lei, X.Z. Liu, W.Q. Ma, Z. Cao, Y.G. Wang, Y. Ding, Flexible Lithium–Air Battery in Ambient Air with an In Situ Formed Gel Electrolyte, Angew. Chem. Int. Ed. 130 (2018) 16363–16367, https://doi.org/10.1002/ANGE.201810882.
[8] J. Yi, X. Liu, S. Guo, K. Zhu, H. Xue, H. Zhou, Novel Stable gel polymer electrolyte: toward a high safety and long life Li-Air battery, ACS. Appl. Mater. Interfaces 7 (2015) 23798–23804, https://doi.org/10.1021/acsami.5b08462.
[9] C. Zhao, Q. Sun, J. Luo, J. Liang, Y. Liu, L. Zhang, J. Wang, S. Deng, X. Lin, X. Yang, H. Huang, S. Zhao, L. Zhang, S. Lu, X. Sun, 3D porous garnet/gel polymer hybrid electrolyte for safe solid-state Li-O2batteries with long lifetimes, Chem. Mater. 32 (2020) 10113–10119, https://doi.org/10.1021/acs.chemmater.0c03529.
[10] T. Yang, C. Shu, Z. Hou, R. Zheng, P. Hei, M. Li, Z. Ran, Q. Zhang, J. Long, 3D porous network gel polymer electrolyte with high transference number for dendrite-free Li[sbnd]O2 batteries, Solid. State. Ion 343 (2019), https://doi.org/10.1016/j.ssi.2019.115088.

[11] B.S. Vishnugopi, F. Hao, A. Verma, P.P. Mukherjee, Double-edged effect of temperature on lithium dendrites, ACS. Appl. Mater. Interfaces 12 (2020) 23931–23938, https://doi.org/10.1021/acsami.0c04355.
[12] Y. Zhao, L. Wang, Y. Zhou, Z. Liang, N. Tavajohi, B. Li, T. Li, Solid polymer electrolytes with high conductivity and transference number of li ions for li-based rechargeable batteries, Adv. Sci. 8 (2021), https://doi.org/10.1002/advs.202003675.
[13] J. Amici, C. Torchio, D. Versaci, D. Dessantis, A. Marchisio, F. Caldera, F. Bella, C. Francia, S. Bodoardo, Nanosponge-based composite gel polymer electrolyte for safer li-o2 batteries, Polymers 13 (2021), https://doi.org/10.3390/polym13101625.
[14] M.Alvarez Tirado, L. Castro, G. Guzmán-González, L. Porcarelli, D. Mecerreyes, Single- versus dual-ion uv-cross-linked gel polymer electrolytes for Li-O2batteries, ACS. Appl. Energy. Mater. 4 (2021) 295–302, https://doi.org/10.1021/acsaem.0c02255.
[15] M.Z. Kufian, S. Ramesh, A.K. Arof, PMMA-LiTFSI based gel polymer electrolyte for lithium-oxygen cell application, Opt. Mater. (Amst) 120 (2021), https://doi.org/10.1016/j.optmat.2021.111418.
[16] S. Wu, J. Yi, K. Zhu, S. Bai, Y. Liu, Y. Qiao, M. Ishida, H. Zhou, A super-hydrophobic quasi-solid electrolyte for Li-O2 battery with improved safety and cycle life in humid atmosphere, Adv. Energy. Mater. 7 (2017), https://doi.org/10.1002/aenm.201601759.
[17] D. Yu, X. Li, J. Xu, Safety regulation of gel electrolytes in electrochemical energy storage devices, Sci. China. Mater. 62 (2019) 1556–1573, https://doi.org/10.1007/s40843-019-9475-4.
[18] G.A. Elia, J. Hassoun, A gel polymer membrane for lithium-ion oxygen battery, Solid. State. Ion 287 (2016) 22–27, https://doi.org/10.1016/j.ssi.2016.01.043.
[19] H. Zhang, S. Wang, A. Wang, Y. Li, F. Yu, Y. Chen, Polyethylene glycol-grafted cellulose-based gel polymer electrolyte for long-life Li-ion batteries, Appl. Surf. Sci. 593 (2022), https://doi.org/10.1016/j.apsusc.2022.153411.
[20] Y.B. Kim, I.T. Kim, M.J. Song, M.W. Shin, Poly-vinylidene-fluoride/p-benzoquinone gel polymer electrolyte with good performance by redox mediator effect for Li-Air battery, Electrochim. Acta 210 (2016) 821–828, https://doi.org/10.1016/j.electacta.2016.06.016.
[21] J. Evanovich, L. King, Hardcore twenty-four : a Stephanie Plum novel, n.d.
[22] C. Zhao, J. Liang, Q. Sun, J. Luo, Y. Liu, X. Lin, Y. Zhao, H. Yadegari, M.N. Banis, R. Li, H. Huang, L. Zhang, R. Yang, S. Lu, X. Sun, Ultralong-life quasi-solid-state Li-O2 batteries enabled by coupling advanced air electrode design with Li metal anode protection, Small. Methods 3 (2019), https://doi.org/10.1002/smtd.201800437.
[23] M. Rayung, M.M. Aung, S.C. Azhar, L.C. Abdullah, M.S. Su'ait, A. Ahmad, S.N.A. M. Jamil, Bio-based polymer electrolytes for electrochemical devices: Insight into the ionic conductivity performance, Materials 13 (2020), https://doi.org/10.3390/ma13040838.
[24] S. Monisha, T. Mathavan, S. Selvasekarapandian, A. Milton Franklin Benial, G. Aristatil, N. Mani, M. Premalatha, D. Vinoth pandi, Investigation of bio polymer electrolyte based on cellulose acetate-ammonium nitrate for potential use in electrochemical devices, Carbohydr. Polym. 157 (2017) 38–47, https://doi.org/10.1016/j.carbpol.2016.09.026.
[25] L. Shi, G. Wang, J. Li, M. Wu, Z. Wen, Sulfonated bacterial cellulose-based functional gel polymer electrolyte for Li-O2Batteries with LiI as a redox mediator, ACS. Sustain. Chem. Eng. 9 (2021) 13883–13892, https://doi.org/10.1021/acssuschemeng.1c05070.
[26] D.F. Vieira, C.O. Avellaneda, A. Pawlicka, Conductivity study of a gelatin-based polymer electrolyte, Electrochim. Acta 53 (2007) 1404–1408, https://doi.org/10.1016/j.electacta.2007.04.034.
[27] C. Li, C. Mu, W. Lin, Novel hemocompatible nanocomposite hydrogels crosslinked with methacrylated gelatin, RSC. Adv 6 (2016) 43663–43671, https://doi.org/10.1039/c6ra04609f.
[28] C. Noè, M. Zanon, A. Arencibia, M.J. López-Muñoz, N.F. de Paz, P. Calza, M. Sangermano, UV-cured chitosan and gelatin hydrogels for the removal of As(V) and Pb(II) from water, Polymers 14 (2022), https://doi.org/10.3390/polym14061268.
[29] F.R. Spectroscopy, T.S.A. Beckert, Electron beam curing of methacrylated gelatin studied, 1997.
[30] B. Velasco- Rodriguez, T. Diaz-vidal, L.C. Rosales-rivera, C.A. García-gonzález, C. Alvarez-lorenzo, A. Al-modlej, V. Domínguez-arca, G. Prieto, S. Barbosa, J.F. A. Soltero Martínez, P. Taboada, Hybrid methacrylated gelatin and hyaluronic acid hydrogel scaffolds. Preparation and systematic characterization for prospective tissue engineering applications, Int. J. Mol. Sci. 22 (2021), https://doi.org/10.3390/ijms22136758.
[31] Z. Wang, Z. Tian, F. Menard, K. Kim, Comparative study of gelatin methacrylate hydrogels from different sources for biofabrication applications, Biofabrication 9 (2017), https://doi.org/10.1088/1758-5090/aa83cf.
[32] M. Zhou, B.H. Lee, Y.J. Tan, L.P. Tan, Microbial transglutaminase induced controlled crosslinking of gelatin methacryloyl to tailor rheological properties for 3D printing, Biofabrication 11 (2019), https://doi.org/10.1088/1758-5090/ab063f.
[33] N. Celikkin, S. Mastrogiacomo, J. Jaroszewicz, X.F. Walboomers, W. Swieszkowski, Gelatin methacrylate scaffold for bone tissue engineering: The influence of polymer concentration, J. Biomed. Mater. Res. A 106 (2018) 201–209, https://doi.org/10.1002/jbm.a.36226.
[34] L. Li, C. Lu, L. Wang, M. Chen, J. White, X. Hao, K.M. McLean, H. Chen, T. C. Hughes, Gelatin-based photocurable hydrogels for corneal wound repair, ACS. Appl. Mater. Interfaces 10 (2018) 13283–13292, https://doi.org/10.1021/acsami.7b17054.
[35] J. Hassoun, P. Reale, B. Scrosati, Recent advances in liquid and polymer lithium-ion batteries, J. Mater. Chem. 17 (2007) 3668–3677, https://doi.org/10.1039/b707040n.
[36] M. Tang, J.C. Chang, S.R. Kumar, S.J. Lue, Glyme-based electrolyte formulation analysis in aprotic lithium-oxygen battery and its cyclic stability, Energy 187 (2019), https://doi.org/10.1016/j.energy.2019.115926.
[37] E. Knipping, C. Aucher, G. Guirado, L. Aubouy, Suitability of blended ionic liquid-dimethylsulfoxide electrolyte for lithium-oxygen battery, Batter. Supercaps 2 (2019) 200–204, https://doi.org/10.1002/batt.201800078.
[38] B. Li, Y. Liu, X. Zhang, P. He, H. Zhou, Hybrid polymer electrolyte for Li–O2 batteries, Green. Energy. Environ. 4 (2019) 3–19, https://doi.org/10.1016/j.gee.2018.08.002.
[39] H. Huo, X. Li, Y. Chen, J. Liang, S. Deng, X. Gao, K. Doyle-Davis, R. Li, X. Guo, Y. Shen, C.W. Nan, X. Sun, Bifunctional composite separator with a solid-state-battery strategy for dendrite-free lithium metal batteries, Energy. Storage. Mater. 29 (2020) 361–366, https://doi.org/10.1016/j.ensm.2019.12.022.
[40] B. Han, P. Jiang, S. Li, X. Lu, Functionalized gel polymer electrolyte membrane for high performance Li metal batteries, Solid. State. Ion 361 (2021), https://doi.org/10.1016/j.ssi.2021.115572.
[41] X. Ye, W. Xiong, T. Huang, X. Li, Y. Lei, Y. Li, X. Ren, J. Liang, X. Ouyang, Q. Zhang, J. Liu, A blended gel polymer electrolyte for dendrite-free lithium metal batteries, Appl. Surf. Sci. 569 (2021), https://doi.org/10.1016/j.apsusc.2021.150899.
[42] X. Liu, X. Xin, L. Shen, Z. Gu, J. Wu, X. Yao, Poly(methyl methacrylate)-based gel polymer electrolyte for high-performance solid state Li-O2battery with enhanced cycling stability, ACS. Appl. Energy. Mater. 4 (2021) 3975–3982, https://doi.org/10.1021/acsaem.1c00344.
[43] N. Meng, F. Lian, Y. Li, X. Zhao, L. Zhang, S. Lu, H. Li, Exploring PVFM-Based Janus Membrane-Supporting Gel Polymer Electrolyte for Highly Durable Li-O2 Batteries, ACS. Appl. Mater. Interfaces 10 (2018) 22237–22247, https://doi.org/10.1021/acsami.8b05393.
[44] Y. Wang, X. Zhu, P. Tan, Y. Wu, Z. Man, X. Wen, Z. Lü, Safe and energy-dense flexible solid-state lithium-oxygen battery with a structured three-dimensional polymer electrolyte, ACS. Sustain. Chem. Eng. 10 (2022) 4894–4903, https://doi.org/10.1021/acssuschemeng.1c07996.
[45] Z. Xu, D. Guo, Z. Liu, Z. Wang, Z. Gu, D. Wang, X. Yao, Cellulose acetate-based high-electrolyte-uptake gel polymer electrolyte for semi-solid-state lithium-oxygen batteries with long-cycling stability, Chem. Asian. J, 17 (2022), https://doi.org/10.1002/asia.202200712.
[46] M. Alvarez-Tirado, L. Castro, A. Guéguen, D. Mecerreyes, Iongel soft solid electrolytes based on [DEME][TFSI] ionic liquid for low polarization lithium-O2 batteries, Batter. Supercaps 5 (2022), https://doi.org/10.1002/batt.202200049.
[47] Y. Chen, M. Yue, C. Liu, H. Zhang, Y. Yu, X. Li, H. Zhang, Long cycle life lithium metal batteries enabled with upright lithium anode, Adv. Funct. Mater 29 (2019), https://doi.org/10.1002/adfm.201806752.
[48] J.S. Jang, M.C. Kim, J.H. Kim, D.H. Park, S.N. Lee, Y.Y. Park, M.H. Kim, J.H. Byeon, J.I. Sohn, K.W. Park, Development of a lithium-oxygen battery with an improved redox mediator applicable to gel polymer electrolytes, J. Ind. Eng. Chem. 117 (2023) 220–226, https://doi.org/10.1016/j.jiec.2022.10.007.
[49] T. Liu, S. Zhao, Q. Xiong, J. Yu, J. Wang, G. Huang, M. Ni, X. Zhang, Reversible discharge products in Li–Air batteries, Adv. Mater. 35 (2023), https://doi.org/10.1002/adma.202208925.
[50] W. Jiao, Q. Su, J. Ge, S. Dong, D. Wang, M. Zhang, S. Ding, G. Du, B. Xu, Mo2C quantum dots decorated ultrathin carbon nanosheets self-assembled into nanoflowers toward highly catalytic cathodes for Li-O2 batteries, Mater. Res. Bull 133 (2021), 111020, https://doi.org/10.1016/j.materresbull.2020.111020.
[51] G. Sun, Q. Zhao, T. Wu, W. Lu, M. Bao, L. Sun, H. Xie, J. Liu, 3D foam-like composites of Mo 2 C nanorods coated by N-Doped carbon: a novel self-standing and binder-free O 2 electrode for Li–O 2 Batteries, ACS. Appl. Mater. Interfaces 10 (2018) 6327–6335, https://doi.org/10.1021/acsami.7b17795.
[52] H. Yu, K.N. Dinh, Y. Sun, H. Fan, Y. Wang, Y. Jing, S. Li, M. Srinivasan, Q. Yan, Performance-improved Li-O 2 batteries by tailoring the phases of Mo x C porous nanorods as an efficient cathode, Nanoscale 10 (2018) 14877–14884, https://doi.org/10.1039/C8NR04319A.
[53] X. Wu, B. Niu, H. Zhang, Z. Li, H. Luo, Y. Tang, X. Yu, L. Huang, X. He, X. Wang, Y. Qiao, S.G. Sun, Enhancing the reaction kinetics and reversibility of Li–O2 batteries by multifunctional polymer additive, Adv. Energy. Mater. 13 (2023), https://doi.org/10.1002/aenm.202203089.